EFFECTS OF 3D REBINNING PROCEDURES ON PET RECONSTRUCTED IMAGES

M. Butti*, E. De Bernardi*, F. Zito**, L. Mainardi*, S. Cerutti*, P. Gerundini**, G. Baselli*

*Department of Biomedical Engineering, Polytechnic University of Milan, Italy
** Nuclear Medicine Department, Ospedale Maggiore Policlinico, Mangiagalli e Regina Elena, Milan, Italy

michele.butti@polimi.it

Abstract: In this work we compared the resolution properties of three 3-D rebinning algorithms when followed by a reconstruction with a classical two-dimensional filtered-backprojection algorithm for positron emission tomography (PET) imaging. We evaluated Fourier rebinning (FORE), multi slice rebinning (MSRB) and single slice rebinning (SSRB), compared also with a 2-D acquisition with transaxial septa. In order to obtain point spread function (PSF) quantifications for axial, tangential and radial direction, we scanned linear sources parallel and perpendicular to the scanner axis and in different positions within the field of view (FOV). The estimated PSF (FWHM) in the transaxial plane after rebinning did not display any significant difference from a 2-D acquisition, both in radial and tangential direction and at any radial displacement. In the axial direction FORE rebinning displayed the best performance with both low blurring and low noise enhancement.

Introduction

In recent years oncological applications of FDG-PET analysis require constantly increasing levels of spatial resolution, sensitivity, contrast recovery and image quality for lesion detectability and quantification. On the other hand, clinical requirements of low dose levels and short scanning and image reconstruction times have to be matched. Acquisition of data in three dimensional (3-D) modality without septa between detector rings allows to record coincidences between pairs of detectors belonging not only to the same ring but also to different rings displaced at several centimeters between each other and connected by oblique line of responses (LORs). In 2-D mode these coincidences would be lost, it is therefore clear the significant improvement in the scanner sensitivity. In this way, for a given acquisition time, 3-D scanning can yield sinograms at higher statistic (roughly 4-5 times), which means that reconstructed images also can have improved statistical accuracy. For the same reasons, for a given statistic we can obtain the same results by injecting a lower level of activity in the patient or performing scanning with shorter acquisition times. However, full explotation of oblique LORs would require the utilization of fully 3-D reconstruction techniques. These techniques are clearly more complex than a 2-D algorithm but, most of all, due to the increased number of LORs, they require a computational time not suited to clinical application. To overcame this problem we can project the oblique LORs into a 2-D sinogram with a fast rebinning procedure and then perform a 2-D image reconstruction on the transaxial sinogram with augmented statistics. However, rebinning approximations can degrade image quality and introduce distortions in the scanner point spread function. Many authors [1]-[3] compared the relative performance of fully 3-D reconstruction methods and different rebinning algorithms followed by FBP or iterative image reconstruction (OSEM); however, this was done without a full characterization of position and direction dependent PSF properties.

In this work we wanted to obtain a careful evaluation of the resolution characteristics of the CTI Siemens ECAT EXACT HR+ scanner within the FOV for the three most widely used rebinning procedures [4], aiming at the inclusion of a reliable space variant PSF model in the system matrix of 2-D numerical reconstruction algorithms (e.g. OSEM) with resolution recovery [5].

Materials and Methods

Data Acquisition: A CTI Siemens ECAT EXACT HR+ scanner was evaluated by means of scans of line sources. The system is a multiring scanner consisting of 32 detector rings; each detector ring consists of 576 bismuth germanate (BGO) crystals with axial and transaxial pitch of 4.39 and 4.05mm, respectively. Data acquisition was performed in 3-D mode, with maximum ring difference 22 and span 9. For the HR+ scanner the number of angles of view is 288, with 144 detectors/angle of view. The transaxial scanner field of view is 58.8cm, while the axial field of view is 15cm containing 63 transaxial slices. Data with similar inclination angles are grouped in 5 segments (see Fig.1). Segment 0 includes data with low inclination angles, and is very similar to the 2-D acquisition, though performed without septa.

Data were obtained from acquisitions of a linear source consisting in a glass capillar, 1mm in inner diameter, 9 cm long. The capillars was filled with an aqueous

ISSN: 1727-1983

solution of ^{18}F-fluorodeoxyglucose (FDG) tracer, with initial activity 37 MBq.

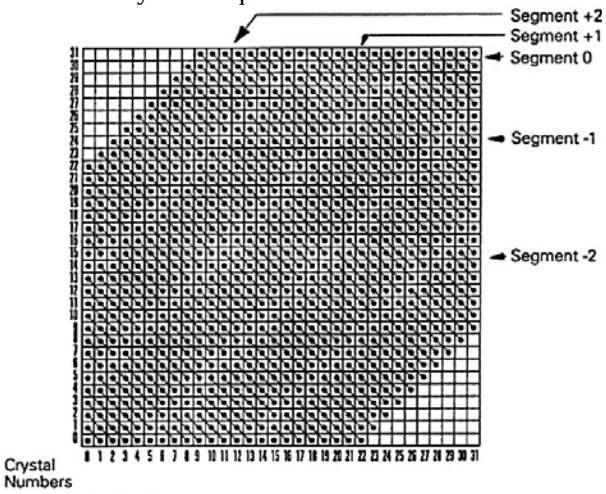

Figure 1: Michelogram for Ring Difference of 22 and Span of 9.

Transaxial PSFs were evaluated in the radial and tangential directions. In order to obtain them, the line source was positioned parallel to the scanner axis and nine acquisitions at different radial distances were performed: 1cm, 5cm, 10cm, 15cm, 18cm, 20cm, 22cm, 24cm, 25cm. Each acquisition lasted 180 sec. Nine different slices starting from the scanner centre were considered from each acquisition in order to assess the PSF. In order to obtain axial PSFs, a single line source was positioned on a radius of a transaxial plane covering the following radial displacement ranges in three subsequent acquisitions: from 0 to 6.75 cm, from 8.775 to 15.525 cm, from 17.55 to 24.3 cm; hence, the broadening over adjacent planes was measured. Two transaxial planes were evaluated, as to axial blurring: the central one and a plane shifted 4 cm from the centre. Each of these acquisitions lasted 240 sec, to compensate for a decrease of activity compared with previous acquisitions.

Prior to perform rebinning and image reconstruction, the standard corrections were applied to the 3-D acquisition data: scatter, random coincidences, detector efficiency, attenuation effects, and geometric aspects.

Reconstruction algorithms: In this work, three well known rebinning algorithms were compared: rebinning Single-Slice (SSRB) [6], rebinning Multi-Slice (MSRB) [7] and the rebinning FORE [8]-[9].

SSRB: the simplest way to reorganize the data is to neglect the inclination angle between the oblique LORs and the transaxial plane and add them to the corresponding transaxial LOR, thus enhancing the direct sinogram midway between the two detector rings involved. This method is very simple and low time consuming but not particularly thorough and can generate a large amount of errors and axial blurring for large inclination angles and distances from the scanner axis. In fact this kind of rebinning is used in applications involving a limited FOV.

MRSB is almost as fast as the previous method but with a better precision and less error: the coincidences of one oblique LOR are added, with a weight matrix, to all planes intersected by the LOR itself. Axial blurring is next corrected with a deconvolution filter, which is based on a probability distribution function (1) of a point source over the slices:

$$q = H \cdot p \tag{1}$$

where q is the set of blurred sinograms, p is the set of ideal (non blurred sinograms) and H is the matrix describing the blurring effects. The estimation of p is then done in an iterative way (2):

$$p^{(k+1)} = p^{(k)} \cdot \left[q \Big/ \left(H \cdot p^{k} \right) \right] \tag{2}$$

In our application, data changed significantly until the 8th iteration, so we stopped the filtering at this level. This technique too imply errors increasing with radial position.

The third algorithm analysed is FORE, obtained from a first order approximation of an exact rebinning formula. Briefly, we can describe the algorithm by the relationship (3):

$$P(\omega, k, z, \delta) \approx P\left(\omega, k, z - \frac{k\delta}{\omega}, 0 \right) \tag{3}$$

where $P(\omega, k)$ is a Fourier transform of a generic sinogram (ω and k are the linear and angular frequency respectively), z is the coordinate in the direction of the scanner axis, δ is the inclination angle. The Fourier transform values of an oblique sinogram is added to the Fourier transform of a transaxial sinogram shifted along the z-direction. Finally, we obtain the rebinned sinogram performing an inverse Fourier transform. This method is more complex than the previous two but can achieve more precise results in a relatively low computational time.

Each set of 3-D rebinned data and 2-D direct data was then reconstructed slice by slice using a classical 2-D filtered-backprojection (FBP) method with an un-windowed ramp filter for successive blurring evaluation on the reconstructed transaxial planes and in the axial direction.

Results

Transactial resolution: In the following the PSF in transaxial planes at different radial displacements r is presented by means of radial and tangential FWHM values. Diagrams of tangential and radial values are displayed in Fig.2 and Fig.3 respectively, showing resolution values at r = 1, 15 and 25 cm off axis. In

ISSN: 1727-1983

order to compare results at different axial positions FWHM estimates are plotted against the different considered planes number from 1 (scanner centre) to 9 (given an image slice thickness of 2.46mm, plane number 9 is placed 19.68mm from the central plane).

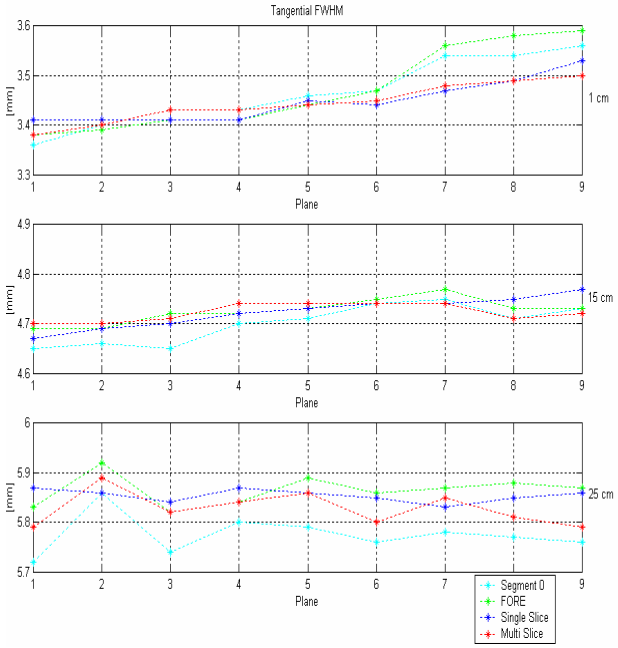

Figure 2: Tangential values of FWHM obtained for different distances from the scanner axis.

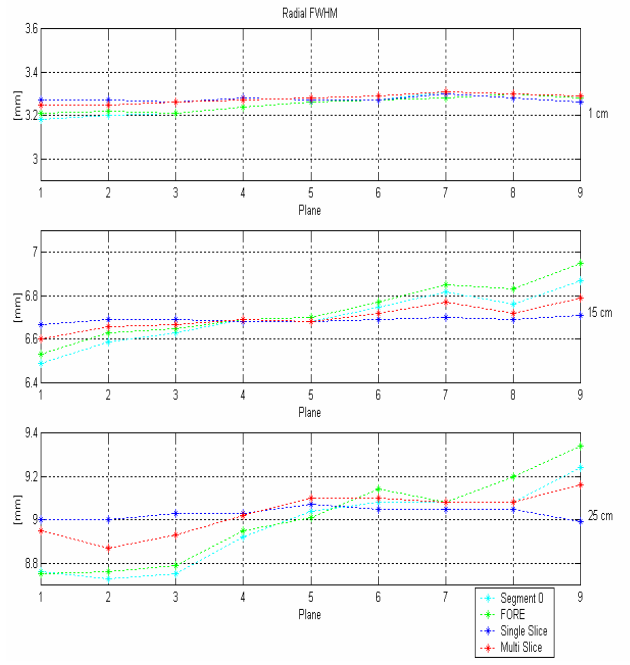

Figure 3: Radial values of FWHM obtained for different distances from the scanner axis.

The diagrams clearly show that negligible differences between transaxial planes were found, as to the considered axial FOV.

A more detailed analysis for the FORE algorithm alone is carried out by Tab.1 and Tab.2, relevant to tangential and radial FWHM values, respectively. In the tables, the per cent variations in comparison to the central plane number 1 are listed.

Table 1: Per cent difference, varying the plane number, of the FWHM values with respect of plane number 1. Tangential data for FORE algorithm.

Tangential		Plane number							
		2	3	4	5	6	7	8	9
Distance of axis	1cm	0,3	0,9	0,9	1,8	2,7	5,3	5,9	6,2
	5cm	0,0	0,0	1,1	1,3	2,4	1,9	2,7	2,4
	10cm	0,5	1,0	1,7	1,2	1,4	1,0	0,0	0,7
	15cm	0,0	0,6	0,6	0,9	1,3	1,7	0,9	0,9
	18cm	0,2	1,0	0,6	1,8	3,3	4,1	3,1	3,3
	20cm	0,8	0,8	0,4	1,2	1,2	1,0	1,2	1,4
	22cm	1,6	1,4	0,7	0,0	0,0	0,2	0,0	0,2
	24cm	0,3	0,2	0,5	0,9	1,7	2,8	2,3	2,1
	25cm	1,5	0,2	0,2	1,0	0,5	0,7	0,9	0,7

Table 2: Per cent difference, varying the plane number, of the FWHM values with respect of plane number 1. Radial data for FORE algorithm.

Radial		Plane number							
		2	3	4	5	6	7	8	9
Distance of axis	1cm	0,3	0,0	0,9	1,6	1,9	2,2	2,8	2,2
	5cm	0,7	0,7	0,9	1,2	6,5	1,2	0,9	0,7
	10cm	1,3	1,3	2,4	1,3	2,4	3,0	3,7	4,7
	15cm	1,5	1,8	2,5	2,6	3,7	4,9	4,6	6,4
	18cm	2,0	2,5	2,7	2,8	4,1	4,4	5,8	6,1
	20cm	1,7	3,4	4,7	5,0	7,9	8,0	6,9	8,8
	22cm	1,5	4,4	6,2	7,2	8,5	9,6	10,7	12,5
	24cm	0,8	1,7	2,9	1,7	2,9	3,9	3,1	3,3
	25cm	0,1	0,5	2,3	3,0	4,5	3,8	5,1	6,7

Little difference is present between planes within the considered axial FOV, slightly more marked in the radial values, increasing with the plane number. The average FWHMs for the nine considered planes is plotted in Fig.4 versus radial position r.

ISSN: 1727-1983

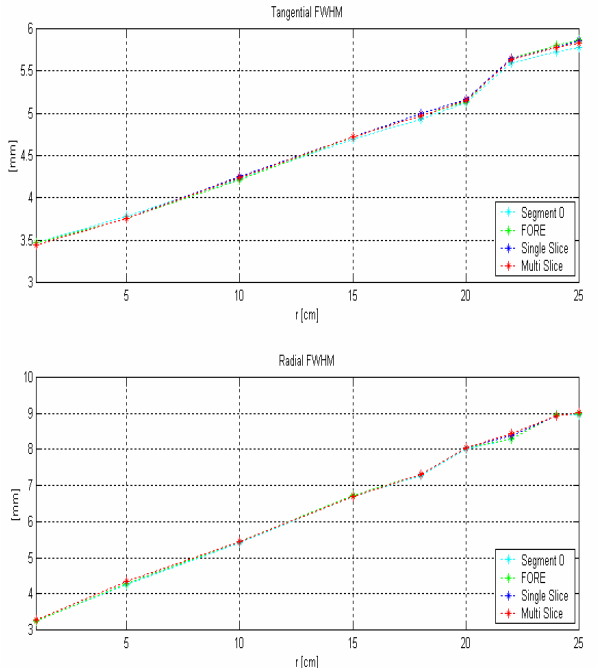

Figure 4: Tangential and Radial values of FWHM obtained for different distance from the scanner axis. Mean values for 9 planes.

As it is well known, resolution displays a nearly linear trend moving from scanner axis to the FOV border. Interestingly, no significant difference between all rebinning algorithms tested in this study is displayed and, furthermore, no increment in blurring appears to be introduced by 3D acquisition plus rebinning in comparison with segment 0, taken as a representative of a 2D acquisition.

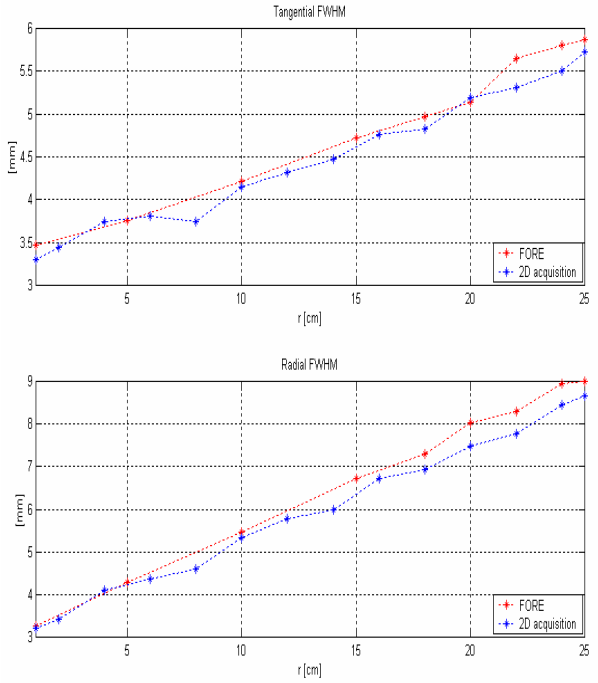

Figure 5: Tangential and Radial values of FWHM for the FORE algorithm and a 2D acquisition.

A more strict comparison of 3D plus rebinning with 2D is carried out in Fig.5, which presents resolution values for rebinning FORE and a real 2D acquisition performed with septa. Similar results were found for the other rebinning methods.

The very limited increment of blurring of 3D which is revealed by this comparison can be explained by the larger presence of scatter in 3D acquisitions. On the contrary, the contribution of rebinning approximations appears to be negligible, as demonstrated by the previous comparison with segment 0.

Axial resolution: In Fig.6 the axial blurring is analysed by displaying FWHM values against radial displacement for the two investigated transaxial planes: central plane and plane with an axial displacement of 4 cm.

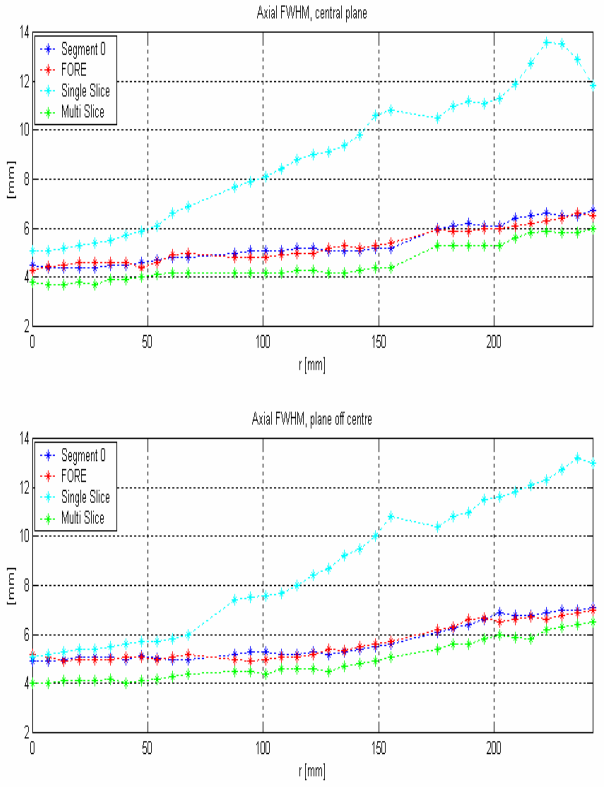

Figure 6: Axial values of FWHM for the two planes investigated.

No significant differences are displayed by the two axial positions. Results confirm the poor performance of the SSRB, even very close to the axis. MSRB would appear slightly better than FORE; however, this is the effect of the resolution recovery provided by the axial filtering final step of the algorithm, that highly raises noise level on the reconstructed image.

Values of FWHM are generally increased with radial displacement. FORE trend is very similar to segment 0; i.e., to the best PSF obtainable without introducing filtering for resolution recovery with the consequent noise enhancement.

ISSN: 1727-1983

Discussion and conclusion

3D PET acquisition can improve acquisition efficiency because of the possibility of taking into account oblique LORs. In order to shorten computational times associated with fully 3D reconstruction techniques it's common to reorganize the 3D data in a set of 2D sinograms by using a rebinning algorithm. In this work the different performances of the three most widely used rebinning methods were analysed: Single-Slice Rebinning (SSRB), Multi-Slice Rebinning (MSRB) and Fourier Rebinning (FORE). Scanning of a linear source for several positions within the field of view and evaluation of the Point Spread Functions for different rebinning at various distances from scanner axis were performed. FWHMs values for tangential, radial and axial resolution were examined.

Results showed that transaxial resolutions do not vary with the rebinning method and that is very similar for the 9 transaxial slices studied in this work.

The Single-Slice method, though valuable for its simplicity and for the modest computational demand, presents values of axial blurring in the range of 10 mm FWHM, about twice the 5 mm displayed by Multi-Slice rebinning and FORE. The difference between Multi-Slice and FORE in terms of axial FWHM is very slight; instead there is difference on the level of noise on the images: the presence of a deconvolution filter in Multi-Slice rebinning allows to obtain low axial values of FWHM but at the same time it elevates the contribution of the noise at high frequencies.

In conclusion this job demonstrates that the application of the rebinning algorithm FORE allows to take advantage of increased statistic, and therefore reduction of the noise, offered from 3D acquisition with an axial blurring (cross-talk between the tomographic plans) comparable to the one offered by the scanner (evalued using data only from segment 0); it demonstrates also that the procedures of rebinning do not degrade the radial and tangential resolutions in the transaxial planes. This results is also important for an easy extension of 2D reconstruction algorithms including a resolution recovery based on blurring models to the rebinned 3D data [5], thus permitting the best compromise among sensitivity, resolution, signal to noise ratio, and computational burden.

References

[1] X. LIU, C. COMTAT, C. MICHEL, P. KINAHAN, M. DEFRISE and D. TOWNSEND (2001): 'Comparison of 3-D Reconstruction With 3D-OSEM and With FORE+OSEM for PET', IEEE Transaction on Medical Imaging, vol.20, no.8, August 2001.

[2] M. DEFRISE, M. SIBOMANA, C. MICHEL and D. NEWPORT (1995): '3D PET reconstruction with the ECAT EXACT HR using Fourier rebinning', IEEE Nuclear Science Symposium and Medical Imaging Conference, vol.3, October 1995.

[3] H. BAGHAEI ,W.H.Wong, J.Uribe, H.Li, Y.Wang, Y.Liu, T.Xing, R.Ramirez, S.Xie, and S.Kim (2004): 'A Comparison of Four-Image Reconstruction Algorithms for 3-D PET Imaging of MDAPET Camera Using Phantom Data', IEEE transactions on nuclear science, vol. 51, no. 5, October 2004.

[4] H. BAGHAEI, J. URIBE, H. LI, Y. WANG and W-H. WONG (2000): 'Comparison of the SSRB, MSRB, and FORE Methods with the 3DRP Algorithm Using Data from a High Resolution PET Scanner', IEEE Nuclear Science Symposium Conference Record, vol.2, October 2000.

[5] BUTTI M., DE BERNARDI E., ZITO F., MAINARDI L., CERUTTI S., GERUNDINI P., BASELLI G. (2004): 'Applying 2D ML iterative reconstruction methods with resolution recovery to 3D PET data: evaluation of rebinning effects', Proc. of the 26th Annual International Conference of the IEEE EMBS San Francisco, CA, USA , September 1-5, 2004, p. 1365-1367

[6] M. E. DAUBE-WITHERSPOON and G. MUEHLLEHNER (1987): 'Treatment of Axial Data in Three-Dimensional PET', *The Journal of Nuclear Medicine*, vol. 28, no.11, November 1987.

[7] R. M. LEWITT, G. MUEHLLEHNER and J. S. KARP (1992): '3D Image Reconstruction for PET by Multi-Slice Rebinning and Axial Filtering', IEEE Nuclear Science Symposium and Medical Imaging Conference, vol.2, October 1992.

[8] MICHEL DEFRISE, P. E. KINAHAN, D. W. TOWNSEND, C. MICHEL, M. SIBOMANA, and D. F. NEWPORT (1997): 'Exact and Approximate Rebinning Algorithms for 3-D PET Data', IEEE Transaction on Medical Imaging, vol.16, no.2, April 1997.

[9] XUAN LIU, MICHEL DEFRISE, CHRISTIAN MICHEL, MÉRENCE SIBOMANA, CLAUDE COMTAT, PAUL KINAHAN, and DAVID TOWNSEND (1999): 'Exact Rebinning Methods for Three-Dimensional PET', IEEE Transaction on Medical Imaging, vol.18, no.8, August 1999.

ISSN: 1727-1983